

Article

Individual Tree Detection from Unmanned Aerial Vehicle (UAV) Derived Canopy Height Model in an Open Canopy Mixed Conifer Forest

Midhun Mohan ^{1,2,*}, Carlos Alberto Silva ³, Carine Klauberg ⁴, Prahlad Jat ⁵, Glenn Catts ¹, Adrián Cardil ⁶, Andrew Thomas Hudak ⁴ and Mahendra Dia ⁷

¹ Department of Forestry and Environmental Resources, North Carolina State University, 2800 Faucette Drive, Raleigh, NC 27695, USA; glenn_catts@ncsu.edu

² Department of Operations Research, North Carolina State University, 2310 Stinson Drive, Raleigh, NC 27695, USA

³ Department of Natural Resources and Society, University of Idaho, 708 South Deakin Street, Moscow, ID 83844, USA; carlos_engflorestal@outlook.com

⁴ USDA Forest Service Rocky Mountain Research Station, Forestry Sciences Laboratory, 1221 South Main Street, Moscow, ID 83843, USA; carine_klauberg@hotmail.com (C.K.); ahudak@fs.fed.us (A.T.H.)

⁵ Department of Environmental Sciences and Engineering, UNC-Chapel Hill, 135 Dauer Drive, Chapel Hill, NC 27599, USA; jat@email.unc.edu

⁶ Tecnosylva, Parque Tecnológico de León, 24009 León, Spain; adriancardil@gmail.com

⁷ Department of Horticultural Sciences, North Carolina State University, 2721 Founders Drive, Raleigh, NC 27695, USA; mdia@ncsu.edu

* Correspondence: mmohan2@ncsu.edu; Tel.: +1-919-771-9348

Received: 28 July 2017; Accepted: 8 September 2017; Published: 11 September 2017

Abstract: Advances in Unmanned Aerial Vehicle (UAV) technology and data processing capabilities have made it feasible to obtain high-resolution imagery and three dimensional (3D) data which can be used for forest monitoring and assessing tree attributes. This study evaluates the applicability of low consumer grade cameras attached to UAVs and structure-from-motion (SfM) algorithm for automatic individual tree detection (ITD) using a local-maxima based algorithm on UAV-derived Canopy Height Models (CHMs). This study was conducted in a private forest at Cache Creek located east of Jackson city, Wyoming. Based on the UAV-imagery, we allocated 30 field plots of 20 m × 20 m. For each plot, the number of trees was counted manually using the UAV-derived orthomosaic for reference. A total of 367 reference trees were counted as part of this study and the algorithm detected 312 trees resulting in an accuracy higher than 85% (*F*-score of 0.86). Overall, the algorithm missed 55 trees (omission errors), and falsely detected 46 trees (commission errors) resulting in a total count of 358 trees. We further determined the impact of fixed tree window sizes (FWS) and fixed smoothing window sizes (SWS) on the ITD accuracy, and detected an inverse relationship between tree density and FWS. From our results, it can be concluded that ITD can be performed with an acceptable accuracy ($F > 0.80$) from UAV-derived CHMs in an open canopy forest, and has the potential to supplement future research directed towards estimation of above ground biomass and stem volume from UAV-imagery.

Keywords: structure from motion (SfM); 3D point cloud; remote sensing; local maxima; fixed tree window size

1. Introduction

Sustainable forest management requires an understanding of how macroscopic patterns of forests emerge, in a timely and accurate manner, in order to make informed decisions [1,2]. Detailed

information on tree-level attributes, such as tree counts, tree heights, crown base heights and diameter at breast height (DBH) are essential for monitoring forest regeneration, quantitative analysis of forest structure and dynamics, and evaluating forest damage [3–6]. However, as several forest study areas are vast and not easily accessible, with a plethora of tree species with varying shapes and sizes, a cost-effective and accurate method to acquire forest attributes such as tree density (tree/ha), and tree characteristics such as height (Ht), basal area (BA), and stem volume (V) are essential to management and conservation activities [7]. Although traditional field surveys can be used to gather detailed information regarding these forest characteristics, they can become uneconomical, time consuming and exhausting, and hence are not ideal for studies dealing with periodic data collection [8,9].

Over the years, remote sensing techniques have been increasingly used for assessing forest resources, both directly and indirectly [10–13]. Aerial photography, light detection and ranging (LiDAR) and airborne multispectral, and hyperspectral images had been perceived as potential tools for observing forest areas and for performing broad-scale analysis of forest systems. These methods have the ability to quantify the composition and structure of the forest at different temporal and geographical scales with the support of various statistical methods, and therefore can supplement forest inventory related expeditions [14–21].

Advances in the fields of the Unmanned Aerial Vehicle (UAV) technology and data processing have broadened the horizons of remote sensing of forestry, and made the acquisition of high-resolution imagery and 3D data more easily available and affordable [22–28]. In fact, UAVs can be obtained at reasonable costs and can be perceived as a forester's eye in the sky, capable of performing forest inventory and analysis on a periodic basis [22,29]. These light-weight machines can be remotely operated from the ground and can fly below cloud cover. With the availability of a wide range of sensors, these UAVs allow the end users to define the spatial resolutions, thereby opening new opportunities to forest managers [30]. In the past decade, studies have focused on exploring the usage of UAV-derived Canopy Height Models (CHMs), suggesting its potential in detection of tree tops, delineation of tree crowns, and subsequently estimation of parameters of crown morphology such as height, diameter, and surface curvature [9,22,23,25,30–32].

Previously, individual trees from UAV imagery were detected using mainly image segmentation using textural features, but photogrammetric 3D point clouds supplanted them with the progression of dense image matching methods and computing power [4,33–39]. For processing large amounts of imaging data, researchers today use so-called structure-from-motion (SfM) and multi-view stereopsis (MVS) techniques, which do not require the information on the 3D position of the camera or the 3D location of multiple control points, unlike traditional digital photogrammetric methods [40–44]. Here, 3D point clouds are generated through the matching of features in multiple images and ground control points (GCPs) are used for geo-referencing and scaling of these point clouds [45]. Nonetheless, very few studies have investigated possibilities of detecting individual tree counts from the CHMs that can be derived from these point clouds [41,46–48].

In the past two decades, LiDAR has become the dominant remote sensing technology for ITD, mainly because it can quickly provide highly accurate and spatially detailed information about forest attributes across an entire forested landscape [7]. There are a variety of approaches used to detect and delineate individual trees from LiDAR-derived CHMs: local maxima detection, valley following (VF), template matching (TM), scale-space (SS) theory, Markov random fields (MRFs), and marked point processes (MPP) [7,35,49–54]. These algorithms, when applied on CHMs derived from aforementioned methodologies, promise efficient ITD performance. For instance, the application of LM algorithm on LiDAR-derived CHMs is a well-known established framework, which has been incorporated in several recent studies and the researchers reported adequate ITD accuracy [7,55]. Nevertheless, these methods were primarily designed for measuring large spaces or objects, and require expensive sensors, well-trained personnel, and precise computational technology to obtain accurate results. Therefore, how to collect high resolution data for individual tree attributes estimation in the case of smaller study areas over time, considering the cost associated with it, is a key challenge [22,23].

As UAV remote sensing techniques are undergoing rapid improvement—along with the availability of high spatial resolution remotely sensed imagery—there is potential for conducting and automating high accuracy forest inventory and analysis in a cost-effective manner [56]. We hypothesize that it is possible to automatically detect individual trees from the UAV-derived CHM with satisfactory accuracy using the LM algorithm, primarily designed for ITD from LiDAR data. In this paper, we aim to address two criteria: (i) Evaluate the applicability of UAV-derived Canopy Height Models for ITD; (ii) Determine the impacts of fixed treetop window size (FWS) and fixed smoothing window size (SWS) on the performance of the local maxima algorithm for ITD.

2. Methods

2.1. Study Area Description

The study area (Figure 1) was comprised of 32 ha of private forest at Cache Creek located east of Jackson city, in the state of Wyoming, with an elevation ranging from 1950 m to 2100 m. The open canopy forest covered about 80% of the total study site and was comprised of a variety of four tree species which included Lodgepole pine (*Pinus contorta* Douglas), Engelmann spruce (*Picea engelmannii* Parry), Subalpine fir (*Abies lasiocarpa* Nuttall) and Douglas fir (*Pseudotsuga menziesii* Franco). The climate of the region was characterized as humid continental climate, with warm to hot summers and cold winters. Annual average precipitation was 33 mm; average temperature ranged from a minimum of $-15\text{ }^{\circ}\text{C}$ in the coolest month (January) to a $27.7\text{ }^{\circ}\text{C}$ in the hottest month (July).

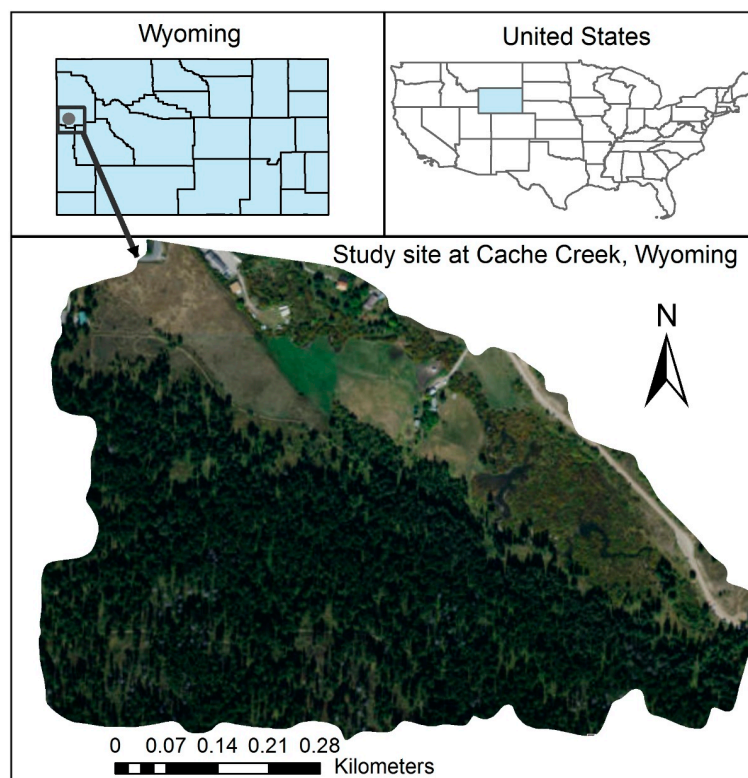


Figure 1. Study Area at Cache Creek, Wyoming, United States of America.

2.2. Data Acquisition and Processing

For this study, the aerial survey was conducted on 13 July 2015 using a DJI phantom 3 quadcopter. It had a compact RGB digital camera—PowerShot S100 (Canon, Tokyo, Japan; zoom lens 5.2 mm; 12.1 Megapixel CMOS sensor; 4000×3000 resolution)—attached to it; the physical dimension of the sensor ($7.5\text{ mm} \times 5.6\text{ mm}$, $1.87\text{ }\mu\text{m}$ pixel size) was 71.5×56.6 degrees. The RGB camera automatically

triggered (1 image/s) during the flight, capturing approximately an area of $14.42 \times 10.77 \text{ m}^2$ with a pixel resolution of 3.5 mm flying at 10 m over the target and was installed on a stabilized gimbal (Photohigher AV200, CARVEC Systems, Hull, UK) along with the spectrometer to reduce the impact of the mechanical vibrations on the scientific instruments.

A total of 383 images from the flights conducted over the study area were used to generate point clouds and CHMs using the Agisoft Photoscan Professional v1.0.0 (www.agisoft.com) software (Agisoft LLC, St. Petersburg, Russia) [57]. Such software implements modern SfM algorithms on RGB photographs and thereby produces 3D reconstruction models based on the location of images with respect to each other as well as to the objects viewed within them [58–61]. In this study, the images had an overlap of 80% which made the stitching process more efficient. The processing steps included automatic aerial triangulation (AAT), bundle block adjustment (BBA), noise filtering, Digital Elevation Model (DEM) and ortho-mosaic creation. All the processes were performed under the default settings and in a fully automated way. The imagery was synchronized using the GPS position, and the ortho-mosaic was generated using absolute GPS coordinates; four random Ground Control Points (GCP) were used for enhancing accuracy. Some specific information of the camera locations and image overlaps related to UAV-image processing conducted in PhotoScan is presented in Table 1.

Table 1. Summary of UAV-image processing using PhotoScan.

Attribute	Value
Number of images	383
Flying altitude	115.29 m
Ground resolution	$0.03 \text{ m} \cdot \text{pix}^{-1}$
Coverage area	0.42 km^{-2}
Camera stations	351
Tie-points	87,635
Error	0.76 pix

The UAV-derived point cloud was used to compute a digital terrain model (DTM) and a CHM. First, ground points were classified using a Progressive Triangulated Irregular Network (TIN) densification algorithm implemented in lasground (settings: step is 10 m, bulge is 0.5 m, spike is 1 m, offset is 0.05 m), LAStools [62], and a 1 m DTM was created using the GridSurfaceCreate functions in FUSION/LDV 3.42 [63]. Afterwards, the UAV-derived point cloud was normalized to height above ground by subtraction of the DTM elevation from the Z coordinate of each point projected on the ground using the ClipData tool. CanopyModel function, also in FUSION/LDV, was used to compute the CHM with 0.5 m of spatial resolution for the study site.

2.3. Individual Tree Identification (ITD)

In this study, we used the local maximum (LM) algorithm [56,64,65], implemented in the rLiDAR package in R [56,64] for ITD on the UAV-derived CHM. FindTreesCHM function was used for automatic detection of tree tops. This function is based on the LM algorithm and it offers an option to search for tree tops in the CHM via a moving window with a fixed tree window size (FWS). To achieve optimal tree detection, we tested four FWS (3×3 , 5×5 , 7×7 and 9×9 pixels) first on an unsmoothed CHM, and then on smoothed CHM by a mean smooth filter with fixed smoothing window sizes (SWS) of 3×3 , 5×5 and 7×7 pixels.

For validation of the ITD, we selected 30 random plots of 400 m^2 ($20 \text{ m} \times 20 \text{ m}$) area each and performed a comparison between UAV based automatic ITD and an ITD done via independent visual assessment of on the UAV-derived orthomosaic, 3d point cloud and CHM. As the number of plots was considerably small, we randomly allocated the sample plots to enhance the robustness of the workflow. Further, we chose the parameters of FWS and SWS which had the best results in ITD with respect to the reference data and performed accuracy assessment for gaining a better understanding of

the statistical factors and for identifying possible drawbacks. In particular, we evaluated the accuracy in terms of true positive (TP, correct detection), false negative (FN, omission error) and false positive (FP, commission error), as well as with respect to recall (r), precision (p) and F -score (F) as explained in Li et al. [66], using the following equations [67,68]:

$$r = TP / TP + FN \quad (1)$$

$$p = TP / TP + FP \quad (2)$$

$$F = 2 \times r \times p / r + p \quad (3)$$

Here, recall can be viewed as a measure of trees-detected, as it is inversely related to omission error; precision represents a measure of trees that were correctly detected, as it is inversely related to commission error, and F -score represents the harmonic mean of recall and precision, and hence higher p and r values result in higher F -scores. Figure 2 provides an overview of the study methodology.

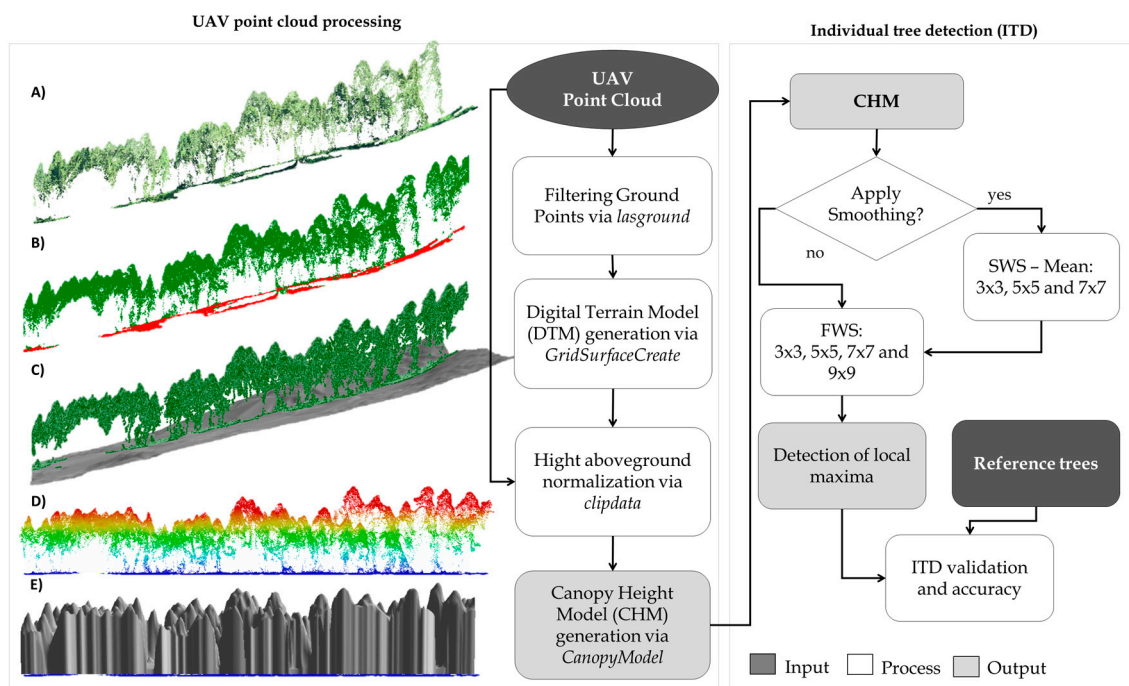


Figure 2. Workflow of the UAV data processing and individual tree detection. (A) UAV-derived point cloud; (B) Classified ground points; (C) Digital Terrain Model (DTM); (D) UAV-point cloud height normalization; (E) Canopy Height Model (CHM).

3. Results

The UAV-derived orthomosaic and CHM are presented in Figure 3. The UAV-derived CHM and LM algorithm proved to be very effective for detecting individual trees in the considered open canopy forest (Table 2; Figures 4 and 5). Importantly, FWS and SWS combinations were found to be a determining factor for the accuracy of ITD (Table 2). FWS of 3×3 and 5×5 are more accurate compared to 7×7 and 9×9 . Lower SWS was found favorable towards ITD success rate as well. Larger SWS resulted in over estimation of tree tops. Finally, we did accuracy assessment on the best combination, which was 3×3 SWS and 3×3 FWS (Table 3).

Table 2. The highlighted grey color represents the best results, which were determined by comparing the number of trees detected (NTD) to the field-based tree inventory number (N). The closest values of NTD compared with N were selected as the best results.

Ref. (FID)	Ref. (N)	Fixed Tree Window Sizes (FWS)															
		3 × 3				5 × 5				7 × 7				9 × 9			
		Smoothing Window Sizes (SWS)															
NF	3 × 3	5 × 5	7 × 7	NF	3 × 3	5 × 5	7 × 7	NF	3 × 3	5 × 5	7 × 7	NF	3 × 3	5 × 5	7 × 7		
1	16	24	12	9	7	13	11	9	6	9	10	8	5	6	8	8	5
2	18	39	17	13	11	22	13	12	9	14	13	9	8	9	8	9	7
3	17	54	22	14	6	22	18	11	6	15	14	8	5	12	10	6	3
4	10	34	12	8	6	12	9	7	5	7	8	6	5	5	6	5	5
5	10	43	11	6	7	17	9	7	4	9	8	5	4	5	4	4	4
6	6	28	6	4	3	10	4	3	3	5	3	3	3	5	3	3	3
7	19	24	13	11	4	15	12	9	4	10	10	9	4	7	8	7	2
8	10	19	13	6	4	5	7	5	4	3	4	4	3	0	2	3	2
9	7	27	6	6	5	9	6	5	5	4	6	5	5	3	6	5	4
10	12	30	12	8	6	9	10	6	5	6	6	5	3	5	5	5	3
11	15	29	12	10	6	15	11	9	6	9	10	8	6	7	9	7	5
12	19	39	19	14	10	21	16	13	8	13	16	12	6	9	11	11	5
13	12	33	10	10	9	13	10	10	8	10	10	10	8	7	10	9	8
14	9	33	9	8	8	15	8	7	7	9	8	7	6	7	7	7	4
15	20	42	19	13	9	18	16	11	5	14	13	10	5	11	11	6	3
16	13	20	13	11	5	13	11	10	5	10	10	10	5	6	10	8	4
17	10	32	10	10	8	14	10	9	7	10	10	9	7	10	10	8	6
18	11	27	11	11	7	13	9	9	4	8	9	8	4	7	10	7	3
19	13	24	13	10	8	13	10	9	7	9	9	9	7	7	9	8	6
20	7	26	7	6	4	10	6	6	4	5	6	5	4	5	5	5	3
21	22	29	17	10	9	17	12	9	6	11	8	8	6	7	8	7	4
22	10	33	11	10	6	15	10	8	5	11	10	7	4	6	7	6	4
23	7	33	7	7	4	15	7	6	4	9	7	4	4	5	5	4	4
24	13	35	15	11	8	13	13	9	6	9	8	7	5	7	7	7	4
25	6	21	5	5	3	6	7	3	3	3	3	3	3	3	2	3	3
26	8	25	9	8	6	10	8	8	5	9	8	8	5	9	7	6	4
27	10	28	11	8	4	16	11	5	4	7	6	3	4	3	5	4	4
28	14	30	14	8	9	12	11	8	6	9	8	7	5	9	8	6	4
29	13	25	12	6	3	11	7	4	3	5	4	4	3	3	3	3	3
30	10	30	10	9	7	14	9	8	6	10	8	6	5	6	7	6	5
Total	367	916	358	270	192	408	301	235	160	262	253	207	147	191	211	183	124

FID: FeatureID; Ref.: reference number of tree per test plot (N); FWS: fixed treetop window size; SWS: fixed smoothing window size; NF: no filter applied.

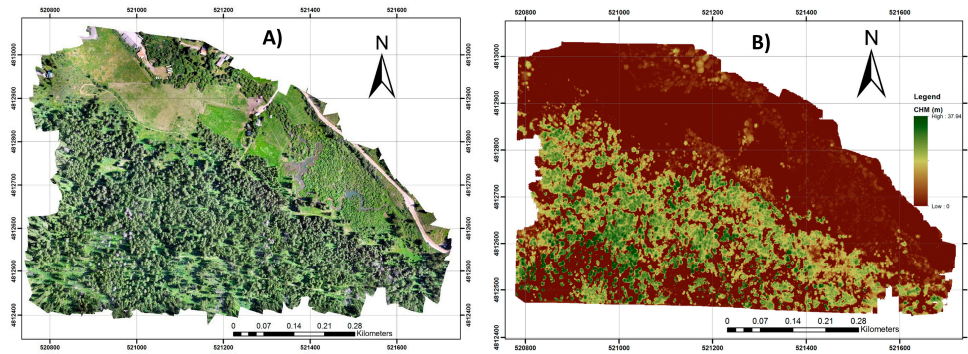


Figure 3. UAV-derived Orthomosaic (A) and Canopy Height Model (B).

For this study, the recall (r) had an overall value of 0.85 with a range of 0.68 to 1.00; overall value of precision (p) was 0.87 with a range of 0.69 to 1.00; and overall value of F -score was 0.86 and it varied from 0.73 to 0.95 (Table 3). Among the 367 reference trees used for this study, 358 (97.55%) trees were detected. In total, the algorithm missed 55 trees, and falsely detected 46 trees, indicating that under detection was higher than over detection.

Table 3. Accuracy assessment results of UAV-based individual tree detection based on False Positive (FP), False Negative (FN), True Positive (TP), recall (r), precision (p) and F -score (F) statistics parameters; where, Ref. (N) is the reference number of trees per test plot.

Ref. (FID)	Ref. (N)	Number of Trees				r	p	F
		UAV	FP	FN	TP			
1	16	12	0	4	12	0.75	1.00	0.86
2	18	17	1	2	16	0.89	0.94	0.91
3	17	22	6	1	16	0.94	0.73	0.82
4	10	12	2	0	10	1.00	0.83	0.91
5	10	11	2	1	9	0.90	0.82	0.86
6	6	6	1	1	5	0.83	0.83	0.83
7	19	13	0	6	13	0.68	1.00	0.81
8	10	13	4	1	9	0.90	0.69	0.78
9	7	6	1	2	5	0.71	0.83	0.77
10	12	12	3	3	9	0.75	0.75	0.75
11	15	12	1	4	11	0.73	0.92	0.81
12	19	19	2	2	17	0.89	0.89	0.89
13	12	10	0	2	10	0.83	1.00	0.91
14	9	9	1	1	8	0.89	0.89	0.89
15	20	19	2	3	17	0.85	0.89	0.87
16	13	13	1	1	12	0.92	0.92	0.92
17	10	10	2	2	8	0.80	0.80	0.80
18	11	11	3	3	8	0.73	0.73	0.73
19	13	13	1	1	12	0.92	0.92	0.92
20	7	7	1	1	6	0.86	0.86	0.86
21	22	17	0	5	17	0.77	1.00	0.87
22	10	11	1	0	10	1.00	0.91	0.95
23	7	7	1	1	6	0.86	0.86	0.86
24	13	15	2	0	13	1.00	0.87	0.93
25	6	5	0	1	5	0.83	1.00	0.91
26	8	9	1	0	8	1.00	0.89	0.94
27	10	11	3	2	8	0.80	0.73	0.76
28	14	14	2	2	12	0.86	0.86	0.86
29	13	12	1	2	11	0.85	0.92	0.88
30	10	10	2	2	8	0.80	0.80	0.80
Total	367	358	47	56	311	0.85	0.87	0.86

The observed and computed tree density in the study area from the UAV-derived CHM were 305 and 300 trees per hectare (TPH; trees·ha⁻¹), respectively. The most accurate results in the ITD were obtained primarily in test subplots with TPH ranging from 150 to 325 trees·ha⁻¹ (Plot FID: 4, 13, 16, 19, 22, 24, 25, 26). On average, 93.2% of trees were detected correctly, with commission and omission errors limited to 8.7% and 6.8%, respectively, with a *F*-score of 0.92. In contrast, the algorithm detected only 81.4% of trees in subplots with TPH > 325 trees·ha⁻¹ with a *F*-score of 0.83. The associated commission and omission errors were 14.4% and 18.6%, respectively.

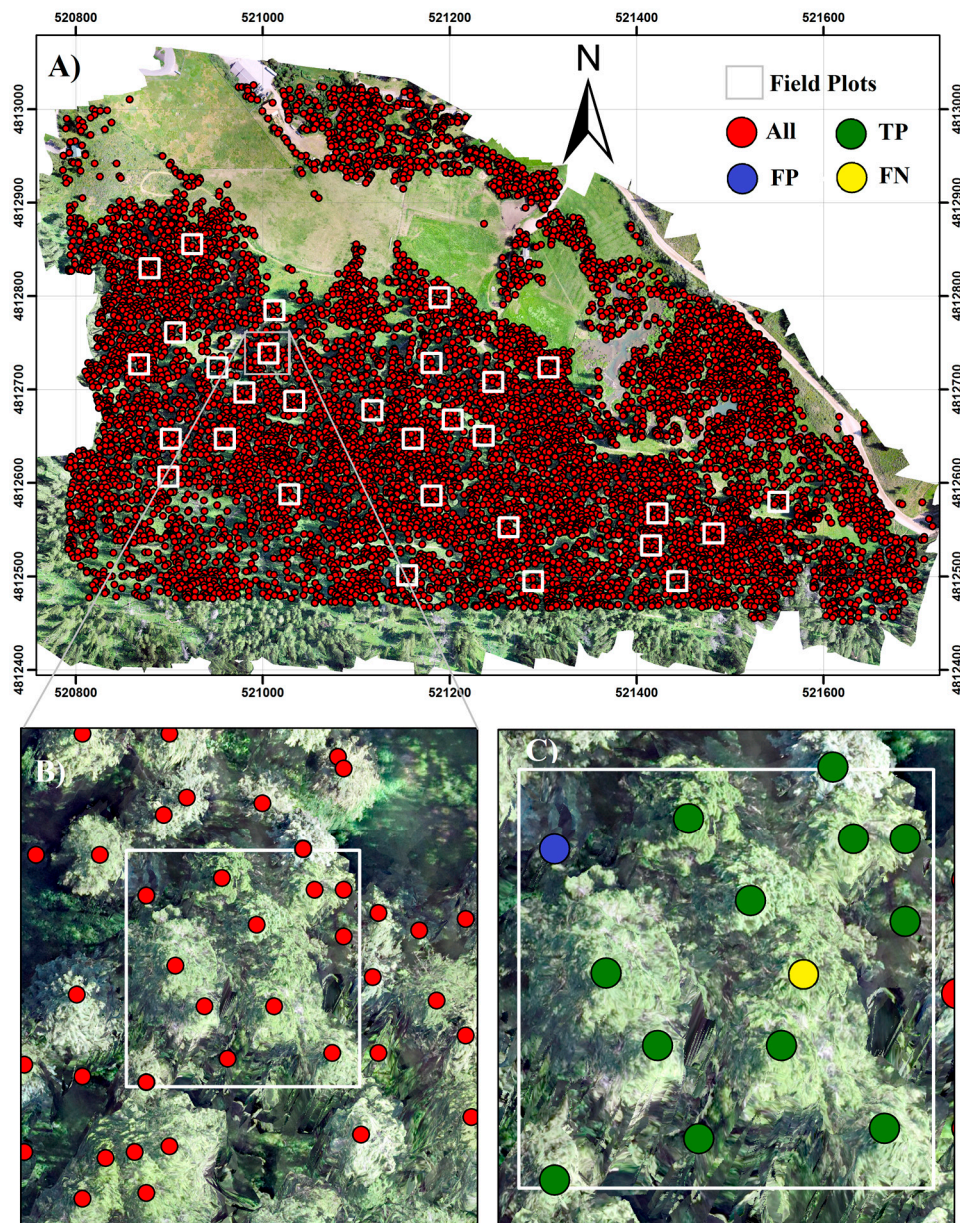


Figure 4. Individual tree detection from UAV-derived Canopy Height Model (CHM). Red dots represent the tree tops detected in the study area at stand level (A), and plot level (Plot 19) (B). Blue and yellow dots represent the commission (FP) and omission (FN) errors while the green dots represent the true positive trees (TP) at the plot 19 and (C).

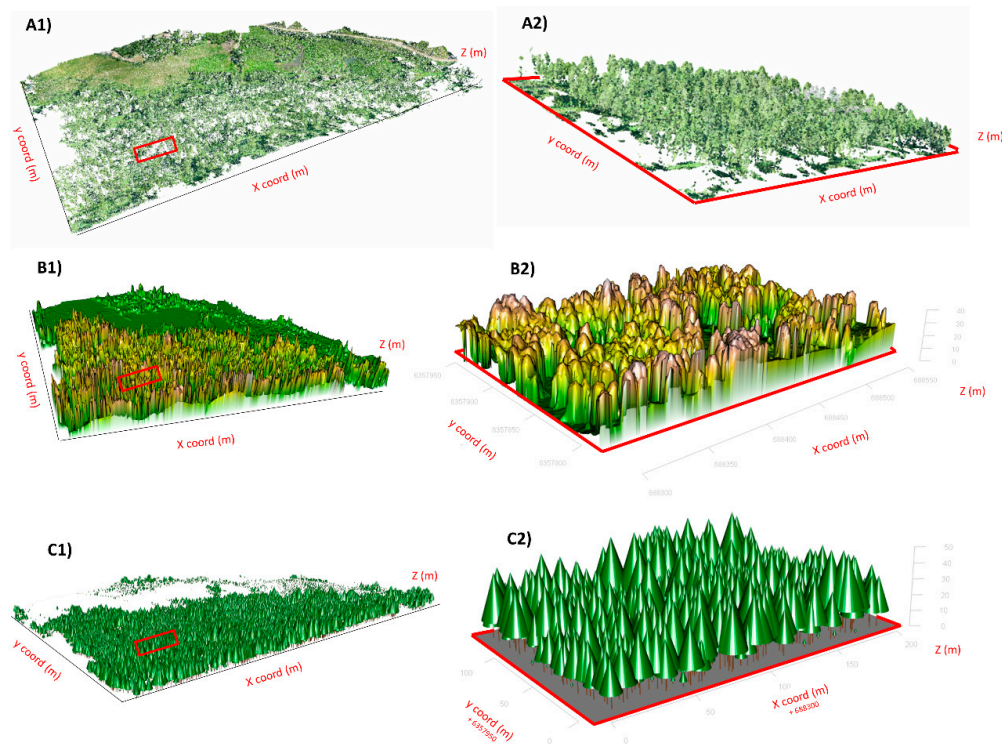


Figure 5. Illustration of individual tree detection at landscape (A1–C1) and plot (A2–C2) scales. (A1,A2) UAV-point cloud; (B1,B2) UAV-derived CHM; (C1,C2) Virtual forest in 3D.

4. Discussion

In the past decade, several studies have highlighted the potential for remote sensing in forestry. In particular, UAV equipped with consumer-grade onboard system camera and different sensors have been used to estimate tree counts, tree heights and crowns measurements due to its low cost and faster performance compared to traditional methods [22,23,69–74]. In this paper, we present a simplified framework for automated ITD from UAV-SfM derived CHM based on algorithms designed for LiDAR data processing. From the perspective of UAV-SfM remote sensing applications, this study can be recognized as a pioneering study for automatic ITD in open canopy mixed conifer forest, which have a comparative efficiency to LiDAR. The presented methodology has the potential to serve as a highly effective, affordable, and easy-to-use approach for ITD and therefore to support forest monitoring and inventory management. Because of the open canopy, we were able to collect sufficient ground points and perform operations similar to LiDAR; the derived data was found to be very detailed and of good quality. Herein, based on our results, it can be stated that UAV-SfM derived CHM coupled with LM algorithm is very capable of deriving tree counts with an acceptable accuracy ($F > 0.80$) in open canopy mixed conifer forests.

The accuracy of ITD in this study was found to be sensitive towards FWS and SWS combinations, and we noticed an inverse relationship between FWS and ITD, as reported by previous studies based on LiDAR data [7]. The most accurate results (i.e., results closest to the observed tree count) for SWS were found at 3×3 irrespective of FWS. Similar results were reported by Silva et al. (2016), where the 3×3 filter eliminated spurious local maxima caused due to irregularity of tree crowns and tree branches. In brief, a consistent FWS parameter can be seen as being more advantageous while performing ITD across a large area. Hence, we chose the best combination, which was 3×3 FWS and 3×3 SWS, for performing accuracy assessment. Even so, it should be borne in mind that the combinations of filter sizes and CHM filter conditions can be affected by forest types and tree size (which is correlated with Tree age) as well [75]. Depending on the intended usage, the users

should always make a trade-off between commission and omission errors, and the overall efficiency of a particular window size can be viewed as a function of the object-resolution relationship which can serve as a first step towards the development of site specific tree identification models. [65]. However, more research pertaining to algorithmic development is needed to develop automated site specific adaptable window size estimations.

Even though we obtained the most accurate results for 3×3 FWS, we observed high commission error in all the cases and on average the algorithm missed around eight trees·ha⁻¹. As the tree detection is based on FWS, having a small FWS results in selection of non-existent trees or multiple trees for an individual tree crown [65]. This further implies that detection of larger trees would be easier as their crown consists of a higher number of pixels compared to the smaller trees. Hence, it is beneficial to have a rough estimate of the threshold tree size beforehand. This inverse relationship between canopy closure and suitable window sizes that we observed in this study was similar to previously reported studies [7,76]. Considering that, the higher success rate of 3×3 can be attributed to denser canopy over the study sites. This would also depend on the diameter and height of the tree species under consideration. In addition, proximity to neighboring trees, trees located under other trees, trees found in shadows or trees having low spectral contrast with respect to understory vegetation are also considered detrimental to tree detection [65]. The overall transferability of our framework can be expected to rely on multiple factors with openness of canopy as one of the most dominant. Hence, the algorithm needs to be continuously improved to adapt to different case scenarios.

In the past decade, several studies have highlighted the potential for using UAV for vegetation mapping on small and large scales [77–80]. However, research in this area is still in its infancy, especially for ITD [70]. Lim et al. [23] identified 11 of 13 trees, with one false positive, utilizing stacked RGB ortho-image and CHM segmentation. Trees not identified possessed small canopies which were not clearly defined from neighboring trees. Sperlich et al. [81] developed point clouds from UAV-based aerial photographs and achieved ITD accuracy of 87.68% within a search radius of 1 m using a pouring algorithm [25]. Kattenborn et al. [25] upgraded Sperlich's algorithm by geometrically classifying UAV-derived point clouds and detected individual palm trees with an overall mapping accuracy of 86.1% for a 9.4 ha study area and 98.2% for dense palm stands. Irrespective of tree detection techniques, heterogeneous stands with mixed and unmanaged trees offer more difficulty in selecting globally optimal segmentation parameters compared to homogenous stands [82]. Changing the crown overlapping threshold could be a viable strategy for determining emergent trees, as crown overlap is a major source for omission errors [83].

Similarly, airborne and terrestrial airborne LiDAR have also been explored for ITD, and have found to provide accurate results depending on forest conditions [84–89]. For instance, Silva et al. (2016), using airborne LiDAR data, found a similar accuracy (F -score > 80) for ITD in longleaf pine forest in Georgia, USA. Maas et al. [86] conducted numerous pilot studies using terrestrial LiDAR and reported that more than 97% of the trees could be detected correctly. Ritter et al. [87] proposed a two-stage density clustering approach for the automatic mapping of tree positions based on terrestrial lidar point cloud data sampled under limited sighting conditions. In their study, the authors detected tree positions in a mixed and vertically structured stand with an overall accuracy of 91.6%, and with omission- and commission error of only 5.7% and 2.7% respectively. Eysn et al. [89] used eight different ITD detection algorithms on airborne LiDAR data of different forest types of Alpine Space and automatically matched the ITD results to forest inventory data. While LiDAR is considered to be a well-suited technology for ITD, the acquisition cost of LiDAR data is still high, which makes the technology impractical for ITD in small areas and over time.

UAV imaging and terrestrial laser scanning systems are appropriate to survey small areas, while airborne laser scanning and hyperspectral systems are mostly used to survey large areas. The area sampled per time unit for these sensors depend of many factors, such as overlap percentage, flight speed, altitude, weather conditions and aim of the study [22,90,91]. UAV-imagery as well as photographs captured by manned aircrafts works differently from LiDAR technologies—whether it be

the process of data extraction or be generation of metrics for assessing forest structure [92–96]. Even so, herein we are showing that the algorithm designed for LiDAR data processing can be also used for the purpose of processing UAV-SfM data ITD. Imaging technology has been found to be more reliable in capturing spectral information of the upper canopy while LiDAR—due to its ability to penetrate into the canopy—is more efficient for vertical stratification of vegetation layers and terrain associated with dense canopies [58,96]. Hence, in the case of close canopy forests, for accurate estimation of tree location and canopy attributes from UAV-SfM, external sources might need to be relied on for supplying DTMs [58,80,95].

While assessing the tree detection capability of our framework, tree location error was not estimated due to data limitations. Nevertheless, we anticipate a possible increase of errors with increasing density of stands, as reported in previous studies [31]. GPS errors associated with tree location estimation is another common source of uncertainty that needs further investigation [95]. Another weakness of this methodology can be attributed to the fact that irregular shapes of tree crowns can be a big problem in high density areas. As shadowing within and between crowns influences canopy reflectance, texture complexity, tree species variety, vertical stand structure and image quality can affect the delineation capacity of the algorithm [82,96–99]. The flight time of small UAVs is also shorter compared to LiDAR, which results in a relatively small sensed area. Even though flying at a higher altitude can be viewed as a remedy, it is detrimental towards the overall accuracy with respect to the resolution (ground sample distance) and it is restricted due to shorter signal range; it might create legal conflicts and privacy issues as well [40,100]. If high density point clouds are to be obtained, the process can become very time consuming. Also, environmental factors such as wind speed, lower visibility due to fog, shadows and temperature variations that can interfere in the efficacy of UAV operations should also be taken into consideration and addressed when working with forest remote sensing, especially for ITD [22,101,102]. Thus, the success rate of the method can be influenced by environmental conditions, existence of different forest types, particularly mixed species, and multilayered forests.

Modern forestry mostly requires forest information in digital format for maintaining a continuous workflow, and UAV based remote sensing offers a promising future in that regard [103,104]. In addition to that, ease of data collection, flexible control of spatial and temporal resolution, low operational costs, and safer work environment underpins the possibility of having a “UAV as a service” data collection market in the foreseeable future. The underlying technological advancement in multi-scale visual mapping, 3D digital modeling and time series analysis using SfM algorithms also empowers research in sectors outside forestry such as construction management [105], water contamination [106], archaeology [107], energy systems [108], computational biology [109] and habitat conservation [110]. Nevertheless, there are a lot of challenges associated with regulated, safe, and comprehensive applications of UAV remote sensing [9]. As multidisciplinary collaborations to promote the standardization of UAV remote sensing development are very limited, upcoming research expeditions should compare themselves with previous studies for systematically determining the optimal UAV remote sensing strategy for given forest lands [9,111]. Formulating methods to increase point density and developing strategies that optimize tree detection algorithms based on the characteristics of the point cloud can surely open new windows in UAV data analytics. Based on the findings presented in this study, future research directions should include species identification and evaluating the accuracy of estimating other tree-level characteristics such as DBH and crown area, which are important factors required for estimating biomass and stem volume.

5. Conclusions

In this study, we investigated the use of consumer grade cameras attached to UAVs and structure-from-motion algorithm for automatic ITD using a local-maxima based algorithm on UAV-derived Canopy Height Models (CHMs). Overall, this research study suggests that LM algorithm combined with proper fixed tree window sizes (FWS) and fixed smoothing window sizes (SWS) is

capable of deriving tree counts with acceptable accuracy ($F > 0.80$) using UAV-derived CHM in open canopy forests. The proposed framework exposes the future potential of UAV-based photogrammetric point clouds for ITD and forest monitoring, and emphasizes that future research should focus on the estimation of individual tree attributes such as tree height, crown size and diameter, and thereby develop predictive models for estimating aboveground biomass and stem volume from UAV-imagery.

Acknowledgments: We would like to thank Joseph Roise, Travis Howell, Stacy Nelson, James McCarter, Siamak Khorram, Trevor Walker, Shalini Shankar, Timur Girgin, and the Department of Environmental Science and Forestry at North Carolina State University for providing the required training, support, facilities and resources to process, analyze and interpret the UAV data.

Author Contributions: All the authors have made substantial contribution towards the successful completion of this manuscript. They all have been involved in designing the study, drafting the manuscript and engaging in critical discussion. M.M., C.A.S, C.K. contributed with the methodological framework, data processing analysis and write up. P.J., G.C., A.C., A.H. and M.D. contributed to the interpretation, quality control and revisions of the manuscript. All authors read and approved the final manuscript.

Conflicts of Interest: The authors declare no conflict of interest.

References

1. Gatzliolis, D.; Lienard, J.F.; Vogs, A.; Strigul, N.S. 3D tree dimensionality assessment using photogrammetry and small unmanned aerial vehicles. *PLoS ONE* **2015**, *10*, e0137765. [[CrossRef](#)] [[PubMed](#)]
2. Cubbage, F.; Roise, J.; Sutherland, R. The Proposed Sale of the Hofmann Forest: A Case Study in Natural Resource Policy. In *Forest Economics and Policy in a Changing Environment: How Market, Policy, and Climate Transformations Affect Forests—Proceedings of the 2016 Meeting of the International Society of Forest Resource Economics*; e-Gen. Tech. Rep. SRS-218; Department of Agriculture Forest Service: Asheville, NC, USA, 2016; p. 81.
3. Kwak, D.A.; Lee, W.K.; Lee, J.H.; Biging, G.S.; Gong, P. Detection of individual trees and estimation of tree height using LiDAR data. *J. For. Res.* **2007**, *12*, 425–434. [[CrossRef](#)]
4. Chen, Q.; Baldocchi, D.; Gong, P.; Kelly, M. Isolating individual trees in a savanna woodland using small footprint lidar data. *Photogramm. Eng. Remote Sens.* **2006**, *72*, 923–932. [[CrossRef](#)]
5. Strigul, N.; Pristinski, D.; Purves, D.; Dushoff, J.; Pacala, S. Scaling from trees to forests: Tractable macroscopic equations for forest dynamics. *Ecol. Monogr.* **2008**, *78*, 523–545. [[CrossRef](#)]
6. Strigul, N. *Individual-Based Models and Scaling Methods for Ecological Forestry: Implications of Tree Phenotypic Plasticity*; INTECH Open Access Publisher: Rijeka, Croatia, 2012.
7. Silva, C.A.; Hudak, A.T.; Vierling, L.A.; Loudermilk, E.L.; O'Brien, J.J.; Hiers, J.K.; Jack, S.B.; Gonzalez-Benecke, C.; Lee, H.; Falkowski, M.J.; et al. Imputation of Individual Longleaf Pine (*Pinus palustris* Mill.) Tree Attributes from Field and LiDAR Data. *Can. J. Remote Sens.* **2016**, *42*, 554–573. [[CrossRef](#)]
8. Gardner, T.A.; Barlow, J.; Araujo, I.S.; Ávila-Pires, T.C.; Bonaldo, A.B.; Costa, J.E.; Esposito, M.C.; Ferreira, L.V.; Hawes, J.; Hernandez, M.I.M.; et al. The cost-effectiveness of biodiversity surveys in tropical forests. *Ecol. Lett.* **2008**, *11*, 139–150. [[CrossRef](#)] [[PubMed](#)]
9. Tang, L.; Shao, G. Drone remote sensing for forestry research and practices. *J. For. Res.* **2015**, *26*, 791–797. [[CrossRef](#)]
10. Hansen, M.C.; Potapov, P.V.; Moore, R.; Hancher, M.; Turubanova, S.A.; Tyukavina, A.; Thau, D.; Stehman, S.V.; Goetz, S.J.; Loveland, T.R.; et al. High-resolution global maps of 21st-century forest cover change. *Science* **2013**, *342*, 850–853. [[CrossRef](#)] [[PubMed](#)]
11. Crowther, T.W.; Glick, H.B.; Covey, K.R.; Bettigole, C.; Maynard, D.S.; Thomas, S.M.; Smith, J.R.; Hintler, G.; Duguid, M.C.; Amatulli, G.; et al. Mapping tree density at a global scale. *Nature* **2015**, *525*, 201–205. [[CrossRef](#)] [[PubMed](#)]
12. Khorram, S.; van der Wiele, C.F.; Koch, F.H.; Nelson, S.A.; Potts, M.D. Remote Sensing: Past and Present. In *Principles of Applied Remote Sensing*; Springer International Publishing: Cham, Switzerland, 2016; pp. 1–20.
13. Roise, J.P.; Harnish, K.; Mohan, M.; Scolforo, H.; Chung, J.; Kanieski, B.; Catts, G.P.; McCarter, J.B.; Posse, J.; Shen, T. Valuation and production possibilities on a working forest using multi-objective programming, Woodstock, timber NPV, and carbon storage and sequestration. *Scand. J. For. Res.* **2016**, *31*, 674–680. [[CrossRef](#)]

14. Waser, L.T.; Baltsavias, E.; Ecker, K.; Eisenbeiss, H.; Ginzler, C.; Kuchler, M.; Thee, P.; Zhang, L. High-resolution digital surface models (DSMs) for modelling fractional shrub/tree cover in a mire environment. *Int. J. Remote Sens.* **2008**, *29*, 1261–1276. [[CrossRef](#)]
15. Wallerman, J.; Bohlin, J.; Fransson, J.E. Forest height estimation using semi-individual tree detection in multi-spectral 3D aerial DMC data. In Proceedings of the 2012 IEEE International Geoscience and Remote Sensing Symposium, Munich, Germany, 22–27 July 2012.
16. Hudak, A.T.; Haren, A.T.; Crookston, N.L.; Liebermann, R.J.; Ohmann, J.L. Imputing forest structure attributes from stand inventory and remotely sensed data in western Oregon, USA. *For. Sci.* **2014**, *60*, 253–269. [[CrossRef](#)]
17. Hansen, E.H.; Gobakken, T.; Bollandsås, O.M.; Zahabu, E.; Næsset, E. Modeling aboveground biomass in dense tropical submontane rainforest using airborne laser scanner data. *Remote Sens.* **2015**, *7*, 788–807. [[CrossRef](#)]
18. Gholizadeh, A.; Mišurec, J.; Kopačková, V.; Mielke, C.; Rogass, C. Assessment of Red-Edge Position Extraction Techniques: A Case Study for Norway Spruce Forests Using HyMap and Simulated Sentinel-2 Data. *Forests* **2016**, *7*, 226. [[CrossRef](#)]
19. Zhang, Z.; Kazakova, A.; Moskal, L.M.; Styers, D.M. Object-based tree species classification in urban ecosystems using LiDAR and hyperspectral data. *Forests* **2016**, *7*, 122. [[CrossRef](#)]
20. Holmgren, J.; Persson, Å. Identifying species of individual trees using airborne laser scanner. *Remote Sens. Environ.* **2004**, *90*, 415–423. [[CrossRef](#)]
21. Silva, C.A.; Klauberg, C.; Hudak, A.T.; Vierling, L.A.; Jaafar, W.S.W.M.; Mohan, M.; Garcia, M.; Ferraz, A.; Cardil, A.; Saatchi, S. Predicting Stem Total and Assortment Volumes in an Industrial *Pinus taeda* L. Forest Plantation Using Airborne Laser Scanning Data and Random Forest. *Forests* **2017**, *8*, 254. [[CrossRef](#)]
22. Zarco-Tejada, P.J.; Diaz-Varela, R.; Angileri, V.; Loudjani, P. Tree height quantification using very high resolution imagery acquired from an unmanned aerial vehicle (UAV) and automatic 3D photo-reconstruction methods. *Eur. J. Agron.* **2014**, *55*, 89–99. [[CrossRef](#)]
23. Lim, Y.S.; La, P.H.; Park, J.S.; Lee, M.H.; Pyeon, M.W.; Kim, J.I. Calculation of Tree Height and Canopy Crown from Drone Images Using Segmentation. *J. Korean Soc. Surv. Geod. Photogramm. Cartogr.* **2015**, *33*, 605–614. [[CrossRef](#)]
24. Torres-Sánchez, J.; López-Granados, F.; Serrano, N.; Arquero, O.; Peña, J.M. High-throughput 3-D monitoring of agricultural-tree plantations with unmanned aerial vehicle (UAV) technology. *PLoS ONE* **2015**, *10*, e0130479. [[CrossRef](#)] [[PubMed](#)]
25. Kattenborn, T.; Sperlich, M.; Bataua, K.; Koch, B. Automatic Single Tree Detection in Plantations using UAV-based Photogrammetric Point clouds. *Int. Arch. Photogramm. Remote Sens. Spat. Inf. Sci.* **2014**, *40*, 139. [[CrossRef](#)]
26. Mlambo, R.; Woodhouse, I.H.; Gerard, F.; Anderson, K. Structure from Motion (SfM) photogrammetry with drone data: A low cost method for monitoring greenhouse gas emissions from forests in developing countries. *Forests* **2017**, *8*, 68. [[CrossRef](#)]
27. Miller, E.; Dandois, J.P.; Detto, M.; Hall, J.S. Drones as a Tool for Monoculture Plantation Assessment in the Steepland Tropics. *Forests* **2017**, *8*, 168. [[CrossRef](#)]
28. Zhang, J.; Hu, J.; Lian, J.; Fan, Z.; Ouyang, X.; Ye, W. Seeing the forest from drones: Testing the potential of lightweight drones as a tool for long-term forest monitoring. *Biol. Conserv.* **2016**, *198*, 60–69. [[CrossRef](#)]
29. Hung, C.; Bryson, M.; Sukkarieh, S. Multi-class predictive template for tree crown detection. *ISPRS J. Photogramm. Remote Sens.* **2012**, *68*, 170–183. [[CrossRef](#)]
30. Wallace, L.; Lucieer, A.; Watson, C.S. Evaluating tree detection and segmentation routines on very high resolution UAV LiDAR data. *IEEE Trans. Geosci. Remote Sens.* **2014**, *52*, 7619–7628. [[CrossRef](#)]
31. Gong, P.; Sheng, Y.; Biging, G.S. 3D model-based tree measurement from high-resolution aerial imagery. *Photogramm. Eng. Remote Sens.* **2002**, *68*, 1203–1212.
32. Song, C. Estimating tree crown size with spatial information of high resolution optical remotely sensed imagery. *Int. J. Remote Sens.* **2007**, *28*, 3305–3322. [[CrossRef](#)]
33. Sumnall, M.J.; Hill, R.A.; Hinsley, S.A. Comparison of small-footprint discrete return and full waveform airborne LiDAR data for estimating multiple forest variables. *Remote Sens. Environ.* **2016**, *173*, 214–223. [[CrossRef](#)]

34. Puliti, S.; Gobakken, T.; Ørka, H.O.; Næsset, E. Assessing 3D point clouds from aerial photographs for species-specific forest inventories. *Scand. J. For. Res.* **2017**, *32*, 68–79. [[CrossRef](#)]
35. Brandtberg, T.; Walter, F. Automated delineation of individual tree crowns in high spatial resolution aerial images by multiple-scale analysis. *Mach. Vis. Appl.* **1998**, *11*, 64–73. [[CrossRef](#)]
36. Wang, L.; Gong, P.; Biging, G.S. Individual tree-crown delineation and treetop detection in high-spatial-resolution aerial imagery. *Photogramm. Eng. Remote Sens.* **2004**, *70*, 351–357. [[CrossRef](#)]
37. Strecha, C.; Von Hansen, W.; Van Gool, L.; Fua, P.; Thoennessen, U. On benchmarking camera calibration and multi-view stereo for high resolution imagery. In Proceedings of the 2008 IEEE Conference on Computer Vision and Pattern Recognition, Anchorage, AK, USA, 23–28 June 2008; pp. 1–8.
38. Küng, O.; Strecha, C.; Beyeler, A.; Zufferey, J.C.; Floreano, D.; Fua, P.; Gervais, F. The accuracy of automatic photogrammetric techniques on ultra-light UAV imagery. In Proceedings of the UAV-g 2011-Unmanned Aerial Vehicle in Geomatics, Zurich, Switzerland, 14–16 September 2011; No. EPFL-CONF-168806.
39. Remondino, F.; Barazzetti, L.; Nex, F.; Scaioni, M.; Sarazzi, D. UAV photogrammetry for mapping and 3d modeling—Current status and future perspectives. *Int. Arch. Photogramm. Remote Sens. Spat. Inf. Sci.* **2011**, *38*, C22. [[CrossRef](#)]
40. Tomašík, J.; Mokroš, M.; Saloň, Š.; Chudý, F.; Tunák, D. Accuracy of Photogrammetric UAV-Based Point Clouds under Conditions of Partially-Open Forest Canopy. *Forests* **2017**, *8*, 151. [[CrossRef](#)]
41. James, M.R.; Robson, S. Straightforward reconstruction of 3D surfaces and topography with a camera: Accuracy and geoscience application. *J. Geophys. Res. Earth Surf.* **2012**, *117*. [[CrossRef](#)]
42. Fritz, A.; Kattenborn, T.; Koch, B. UAV-based photogrammetric point clouds—Tree stem mapping in open stands in comparison to terrestrial laser scanner point clouds. *Int. Arch. Photogramm. Remote Sens. Spat. Inf. Sci.* **2013**, *40*, 141–146. [[CrossRef](#)]
43. Haala, N.; Hastedt, H.; Wolf, K.; Ressler, C.; Baltrusch, S. Digital photogrammetric camera evaluation—generation of digital elevation models. *Photogramm.-Fernerkund.-Geoinf.* **2010**, *2010*, 99–115. [[CrossRef](#)] [[PubMed](#)]
44. Baltsavias, E.; Gruen, A.; Eisenbeiss, H.; Zhang, L.; Waser, L.T. High-quality image matching and automated generation of 3D tree models. *Int. J. Remote Sens.* **2008**, *29*, 1243–1259. [[CrossRef](#)]
45. Westoby, M.J.; Brasington, J.; Glasser, N.F.; Hambrey, M.J.; Reynolds, J.M. ‘Structure-from-Motion’ photogrammetry: A low-cost, effective tool for geoscience applications. *Geomorphology* **2012**, *179*, 300–314. [[CrossRef](#)]
46. James, M.R.; Robson, S. Mitigating systematic error in topographic models derived from UAV and ground-based image networks. *Earth Surface Proc. Landforms* **2014**, *39*, 1413–1420. [[CrossRef](#)]
47. Hernández-Clemente, R.; Navarro-Cerrillo, R.M.; Ramírez, F.J.R.; Hornero, A.; Zarco-Tejada, P.J. A novel methodology to estimate single-tree biophysical parameters from 3D digital imagery compared to aerial laser scanner data. *Remote Sens.* **2014**, *6*, 11627–11648. [[CrossRef](#)]
48. Dempewolf, J.; Nagol, J.; Hein, S.; Thiel, C.; Zimmermann, R. Measurement of Within-Season Tree Height Growth in a Mixed Forest Stand Using UAV Imagery. *Forests* **2017**, *8*, 231. [[CrossRef](#)]
49. Kwak, D.A.; Lee, W.K.; Lee, J.H. Predicting forest stand characteristics with detection of individual tree. In Proceedings of the MAPPs/ASPRS 2006 Fall Conference, San Antonio, TX, USA, 6–10 November 2006.
50. Larsen, M.; Eriksson, M.; Descombes, X.; Perrin, G.; Brandtberg, T.; Gougeon, F.A. Comparison of six individual tree crown detection algorithms evaluated under varying forest conditions. *Int. J. Remote Sens.* **2011**, *32*, 5827–5852. [[CrossRef](#)]
51. Lee, J.H.; Biging, G.S.; Fisher, J.B. An Individual Tree-Based Automated Registration of Aerial Images to Lidar Data in a Forested Area. *Photogramm. Eng. Remote Sens.* **2016**, *82*, 699–710. [[CrossRef](#)]
52. Descombes, X.; Pechersky, E. Tree Crown Extraction Using a Three State Markov Random Field. Ph.D. Thesis, INRIA, Rocquencourt, France, 2006.
53. Perrin, G.; Descombes, X.; Zerubia, J. *A Non-Bayesian Model for Tree Crown Extraction Using Marked Point Processes*; INRIA: Rocquencourt, France, 2006.
54. Gougeon, F.A. Automatic individual tree crown delineation using a valley-following algorithm and rule-based system. In Proceedings of the International Forum on Automated Interpretation of High Spatial Resolution Digital Imagery for Forestry, Victoria, BC, Canada, 10–12 February 1998; pp. 11–23.
55. Koch, B.; Heyder, U.; Weinacker, H. Detection of individual tree crowns in airborne lidar data. *Photogramm. Eng. Remote Sens.* **2006**, *72*, 357–363. [[CrossRef](#)]

56. R Core Team. *R: A Language and Environment for Statistical Computing*; R Foundation for Statistical Computing: Vienna, Austria; Available online: <http://www.R-project.org> (accessed on 15 October 2015).
57. AgiSoft, L.L.C. PhotoScan Professional Edition v.1.0.3. Available online: www.agisoft.ru (accessed on 3 October 2015).
58. Dandois, J.P.; Ellis, E.C. High spatial resolution three-dimensional mapping of vegetation spectral dynamics using computer vision. *Remote Sens. Environ.* **2013**, *136*, 259–276. [[CrossRef](#)]
59. Lucieer, A.; Turner, D.; King, D.H.; Robinson, S.A. Using an Unmanned Aerial Vehicle (UAV) to capture micro-topography of Antarctic moss beds. *Int. J. Appl. Earth Obs. Geoinf.* **2014**, *27*, 53–62. [[CrossRef](#)]
60. Turner, D.; Lucieer, A.; Wallace, L. Direct georeferencing of ultrahigh-resolution UAV imagery. *IEEE Trans. Geosci. Remote Sens.* **2014**, *52*, 2738–2745. [[CrossRef](#)]
61. Verhoeven, G. Taking computer vision aloft—Archaeological three-dimensional reconstructions from aerial photographs with photoscan. *Archaeol. Prospect.* **2011**, *18*, 67–73. [[CrossRef](#)]
62. Isenburg, M. LAStools—Efficient Tools for LiDAR Processing. Available online: lastools.org (accessed on 3 October 2015).
63. Kraus, K.; Pfeifer, N. Determination of terrain models in wooded areas with airborne laser scanner data. *ISPRS J. Photogramm. Remote Sens.* **1998**, *53*, 193–203. [[CrossRef](#)]
64. Silva, C.A.; Crookston, N.L.; Hudak, A.T.; Vierling, L.A. rLiDAR: An R Package for Reading, Processing and Visualizing LiDAR (Light Detection and Ranging) Data, Version 0.1. Available online: <http://cran.rproject.org/web/packages/rLiDAR/index.html> (accessed on 15 October 2015).
65. Wulder, M.; Niemann, K.O.; Goodenough, D.G. Local maximum filtering for the extraction of tree locations and basal area from high spatial resolution imagery. *Remote Sens. Environ.* **2000**, *73*, 103–114. [[CrossRef](#)]
66. Li, W.; Guo, Q.; Jakubowski, M.K.; Kelly, M. A new method for segmenting individual trees from the lidar point cloud. *Photogramm. Eng. Remote Sens.* **2012**, *78*, 75–84. [[CrossRef](#)]
67. Goutte, C.; Gaussier, E. A probabilistic interpretation of precision, recall and F-score, with implication for evaluation. In Proceedings of the European Conference on Information Retrieval, Compostela, Spain, 21–23 March 2005; Springer: Berlin/Heidelberg, Germany, 2005; pp. 345–359.
68. Sokolova, M.; Japkowicz, N.; Szpakowicz, S. Beyond accuracy, F-score and ROC: A family of discriminant measures for performance evaluation. In Proceedings of the Australasian Joint Conference on Artificial Intelligence, Auckland, New Zealand, 1–5 December 2008; Springer: Berlin/Heidelberg, Germany, 2008; pp. 1015–1021.
69. Puttock, A.K.; Cunliffe, A.M.; Anderson, K.; Brazier, R.E. Aerial photography collected with a multirotor drone reveals impact of Eurasian beaver reintroduction on ecosystem structure 1. *J. Unmanned Veh. Syst.* **2015**, *3*, 123–130. [[CrossRef](#)]
70. Koh, L.; Wich, S. Dawn of drone ecology: Low-cost autonomous aerial vehicles for conservation. *Trop. Conserv. Sci.* **2012**, *5*, 121–132. [[CrossRef](#)]
71. Paneque-Gálvez, J.; McCall, M.K.; Napoletano, B.M.; Wich, S.A.; Koh, L.P. Small drones for community-based forest monitoring: An assessment of their feasibility and potential in tropical areas. *Forests* **2014**, *5*, 1481–1507. [[CrossRef](#)]
72. Getzin, S.; Wiegand, K.; Schöning, I. Assessing biodiversity in forests using very high-resolution images and unmanned aerial vehicles. *Methods Ecol. Evol.* **2012**, *3*, 397–404. [[CrossRef](#)]
73. Felderhof, L.; Gillieson, D. Near-infrared imagery from unmanned aerial systems and satellites can be used to specify fertilizer application rates in tree crops. *Can. J. Remote Sens.* **2012**, *37*, 376–386. [[CrossRef](#)]
74. Wallace, L.; Watson, C.; Lucieer, A. Detecting pruning of individual stems using airborne laser scanning data captured from an unmanned aerial vehicle. *Int. J. Appl. Earth Obs. Geoinf.* **2014**, *30*, 76–85. [[CrossRef](#)]
75. Lindberg, E.; Hollaus, M. Comparison of methods for estimation of stem volume, stem number and basal area from airborne laser scanning data in a hemi-boreal forest. *Remote Sens.* **2012**, *4*, 1004–1023. [[CrossRef](#)]
76. Falkowski, M.J.; Smith, A.M.; Gessler, P.E.; Hudak, A.T.; Vierling, L.A.; Evans, J.S. The influence of conifer forest canopy cover on the accuracy of two individual tree measurement algorithms using lidar data. *Can. J. Remote Sens.* **2008**, *34* (Suppl. S2), S338–S350. [[CrossRef](#)]
77. Merino, L.; Caballero, F.; Martínez-de-Dios, J.R.; Maza, I.; Ollero, A. An unmanned aircraft system for automatic forest fire monitoring and measurement. *J. Intell. Robot. Syst.* **2012**, *65*, 533–548. [[CrossRef](#)]
78. Martínez-de Dios, J.R.; Merino, L.; Caballero, F.; Ollero, A. Automatic forest-fire measuring using ground stations and unmanned aerial systems. *Sensors* **2011**, *11*, 6328–6353. [[CrossRef](#)] [[PubMed](#)]

79. Ota, T.; Ogawa, M.; Shimizu, K.; Kajisa, T.; Mizoue, N.; Yoshida, S.; Takao, G.; Hirata, Y.; Furuya, N.; Sano, T.; et al. Aboveground biomass estimation using structure from motion approach with aerial photographs in a seasonal tropical forest. *Forests* **2015**, *6*, 3882–3898. [[CrossRef](#)]
80. Panagiotidis, D.; Abdollahnejad, A.; Surový, P.; Chiteculo, V. Determining tree height and crown diameter from high-resolution UAV imagery. *Int. J. Remote Sens.* **2017**, *38*, 2392–2410. [[CrossRef](#)]
81. Sperlich, M.; Kattenborn, T.; Koch, B.; Kattenborn, G. Potential of Unmanned Aerial Vehicle Based Photogrammetric Point Clouds for Automatic Single Tree Detection. Available online: <http://www.dgpf.de/neu/Proc2014/proceedings/papers/Beitrag270.pdf> (accessed on 15 January 2015).
82. La, H.P.; Eo, Y.D.; Chang, A.; Kim, C. Extraction of individual tree crown using hyperspectral image and LiDAR data. *KSCE J. Civ. Eng.* **2015**, *19*, 1078–1087. [[CrossRef](#)]
83. Zhou, J.; Proisy, C.; Descombes, X.; Le Maire, G.; Nouvellon, Y.; Stape, J.L.; Viennois, G.; Zerubia, J.; Couteron, P. Mapping local density of young Eucalyptus plantations by individual tree detection in high spatial resolution satellite images. *For. Ecol. Manag.* **2013**, *301*, 129–141. [[CrossRef](#)]
84. Eysn, L.; Hollaus, M.; Lindberg, E.; Berger, F.; Monnet, J.-M.; Dalponte, M.; Kobal, M.; Pellegrini, M.; Lingua, E.; Mongus, D.; et al. A benchmark of lidar-based single tree detection methods using heterogeneous forest data from the alpine space. *Forests* **2015**, *6*, 1721–1747. [[CrossRef](#)]
85. Astrup, R.; Ducey, M.J.; Granhus, A.; Ritter, T.; von Lüpke, N. Approaches for estimating stand-level volume using terrestrial laser scanning in a single-scan mode. *Can. J. For. Res.* **2014**, *44*, 666–676. [[CrossRef](#)]
86. Maas, H.G.; Bienert, A.; Scheller, S.; Keane, E. Automatic forest inventory parameter determination from terrestrial laser scanner data. *Int. J. Remote Sens.* **2008**, *29*, 1579–1593. [[CrossRef](#)]
87. Ritter, T.; Schwarz, M.; Tockner, A.; Leisch, F.; Nothdurft, A. Automatic Mapping of Forest Stands Based on Three-Dimensional Point Clouds Derived from Terrestrial Laser-Scanning. *Forests* **2017**, *8*, 265. [[CrossRef](#)]
88. Liang, X.; Hyypä, J. Automatic stem mapping by merging several terrestrial laser scans at the feature and decision levels. *Sensors* **2013**, *13*, 1614–1634. [[CrossRef](#)] [[PubMed](#)]
89. Liang, X.; Litkey, P.; Hyypä, J.; Kaartinen, H.; Vastaranta, M.; Holopainen, M. Automatic stem mapping using single-scan terrestrial laser scanning. *IEEE Trans. Geosci. Remote Sens.* **2012**, *50*, 661–670. [[CrossRef](#)]
90. White, J.C.; Wulder, M.A.; Vastaranta, M.; Coops, N.C.; Pitt, D.; Woods, M. The utility of image-based point clouds for forest inventory: A comparison with airborne laser scanning. *Forests* **2013**, *4*, 518–536. [[CrossRef](#)]
91. Whitehead, K.; Hugenholtz, C.H. Remote sensing of the environment with small unmanned aircraft systems (UASs), part 1: A review of progress and challenges. *J. Unmanned Veh. Syst.* **2014**, *2*, 69–85. [[CrossRef](#)]
92. Lin, Y.; Jiang, M.; Yao, Y.; Zhang, L.; Lin, J. Use of UAV oblique imaging for the detection of individual trees in residential environments. *Urban For. Urban Green.* **2015**, *14*, 404–412. [[CrossRef](#)]
93. White, J.C.; Stepper, C.; Tompalski, P.; Coops, N.C.; Wulder, M.A. Comparing ALS and image-based point cloud metrics and modelled forest inventory attributes in a complex coastal forest environment. *Forests* **2015**, *6*, 3704–3732. [[CrossRef](#)]
94. Penner, M.; Woods, M.; Pitt, D.G. A comparison of airborne laser scanning and image point cloud derived tree size class distribution models in boreal Ontario. *Forests* **2015**, *6*, 4034–4054. [[CrossRef](#)]
95. Lisein, J.; Pierrot-Deseilligny, M.; Bonnet, S.; Lejeune, P. A photogrammetric workflow for the creation of a forest canopy height model from small unmanned aerial system imagery. *Forests* **2013**, *4*, 922–944. [[CrossRef](#)]
96. Vauhkonen, J.; Korpela, I.; Maltamo, M.; Tokola, T. Imputation of single-tree attributes using airborne laser scanning-based height, intensity, and alpha shape metrics. *Remote Sens. Environ.* **2010**, *114*, 1263–1276. [[CrossRef](#)]
97. Wing, M.G.; Eklund, A.; John, S.; Richard, K. Horizontal measurement performance of five mapping-grade global positioning system receiver configurations in several forested settings. *West. J. Appl. For.* **2008**, *23*, 166–171.
98. Asner, G.P.; Heidebrecht, K.B. Spectral unmixing of vegetation, soil and dry carbon cover in arid regions: Comparing multispectral and hyperspectral observations. *Int. J. Remote Sens.* **2002**, *23*, 3939–3958. [[CrossRef](#)]
99. Wulder, M.A.; Dechka, J.A.; Gillis, M.A.; Luther, J.E.; Hall, R.J.; Beaudoin, A.; Franklin, S.E. Operational mapping of the land cover of the forested area of Canada with Landsat data: EOSD land cover program. *For. Chron.* **2003**, *79*, 1075–1083. [[CrossRef](#)]
100. Puliti, S.; Ørka, H.O.; Gobakken, T.; Næsset, E. Inventory of small forest areas using an unmanned aerial system. *Remote Sens.* **2015**, *7*, 9632–9654. [[CrossRef](#)]

101. Nevalainen, O.; Honkavaara, E.; Tuominen, S.; Viljanen, N.; Hakala, T.; Yu, X.; Hyyppä, J.; Saari, H.; Pölonen, I.; Imai, N.N.; et al. Individual tree detection and classification with UAV-based photogrammetric point clouds and hyperspectral imaging. *Remote Sens.* **2017**, *9*, 185. [[CrossRef](#)]
102. Dandois, J.P.; Olano, M.; Ellis, E.C. Optimal altitude, overlap, and weather conditions for computer vision UAV estimates of forest structure. *Remote Sens.* **2015**, *7*, 13895–13920. [[CrossRef](#)]
103. Birdal, A.C.; Avdan, U.; Türk, T. Estimating tree heights with images from an unmanned aerial vehicle. *Geomat. Nat. Hazards Risk* **2017**. [[CrossRef](#)]
104. Tang, L.; Shao, G.; Dai, L. Roles of digital technology in China's sustainable forestry development. *Int. J. Sustain. Dev. World Ecol.* **2009**, *16*, 94–101. [[CrossRef](#)]
105. Golparvar-Fard, M.; Peña-Mora, F.; Savarese, S. D4AR—A 4-dimensional augmented reality model for automating construction progress monitoring data collection, processing and communication. *J. Inf. Technol. Constr.* **2009**, *14*, 129–153.
106. Jat, P.; Serre, M.L. Bayesian Maximum Entropy space/time estimation of surface water chloride in Maryland using river distances. *Environ. Pollut.* **2016**, *219*, 1148–1155. [[CrossRef](#)] [[PubMed](#)]
107. Green, S.; Bevan, A.; Shapland, M. A comparative assessment of structure from motion methods for archaeological research. *J. Archaeol. Sci.* **2014**, *46*, 173–181. [[CrossRef](#)]
108. Azadeh, A.; Taghipour, M.; Asadzadeh, S.M.; Abdollahi, M. Artificial immune simulation for improved forecasting of electricity consumption with random variations. *Int. J. Electr. Power Energy Syst.* **2014**, *55*, 205–224. [[CrossRef](#)]
109. Murugesan, S.; Bouchard, K.; Chang, E.; Dougherty, M.; Hamann, B.; Weber, G.H. Multi-scale visual analysis of time-varying electrocorticography data via clustering of brain regions. *BMC Bioinform.* **2017**, *18*, 236. [[CrossRef](#)] [[PubMed](#)]
110. Johnston, A.N.; Moskal, L.M. High-resolution habitat modeling with airborne LiDAR for red tree voles. *J. Wildl. Manag.* **2017**, *81*, 58–72. [[CrossRef](#)]
111. Shahbazi, M.; Théau, J.; Ménard, P. Recent applications of unmanned aerial imagery in natural resource management. *GISci. Remote Sens.* **2014**, *51*, 339–365. [[CrossRef](#)]



© 2017 by the authors. Licensee MDPI, Basel, Switzerland. This article is an open access article distributed under the terms and conditions of the Creative Commons Attribution (CC BY) license (<http://creativecommons.org/licenses/by/4.0/>).